
Classification of Object Point Clouds: A Practical Perspective

Zelin Xu^{*1} Ke Chen^{*1} Changxing Ding¹

Yaowei Wang² Kui Jia¹

¹South China University of Technology ²Peng Cheng Laboratory
eexuzelin@mail.scut.edu.cn wangyw@pcl.ac.cn
{chenk, chxding, kuijia}@scut.edu.cn

Abstract

As a 3D counterpart of object classification in images, object point cloud classification is fundamental to 3D scene understanding, and has drawn great research attention since the release of benchmarking datasets, such as the ModelNet and the ShapeNet. These benchmarks assume point clouds covering *complete* surfaces of object instances, for which plenty of high-performing methods have been developed. However, their settings deviate from those often met in practice, where, due to (self-)occlusion, a point cloud covering *partial* surface of an object is captured from an arbitrary view. We show in this paper that performance of existing point cloud classification methods drops drastically under the considered practical *single-view, partial* setting; the phenomenon is consistent with the observation that semantic category of a partial object surface is less ambiguous only when its distribution on the whole surface is clearly specified. To this end, we argue for a single-view, partial setting where supervised learning of object pose estimation should be accompanied with classification. Technically, we propose a baseline method of *Pose-Accompanied Point cloud classification Network (PAPNet)*; built upon $SE(3)$ -equivariant convolutions, the PAPNet learns intermediate pose transformations for equivariant features defined on vector fields, which makes the subsequent classification easier (ideally) in the category-level, canonical pose. We adapt existing ModelNet40 and ScanNet datasets on point set classification to the introduced *single-view, partial* setting to verify our hypothesis. Thorough experiments confirm the necessity of object pose estimation; our PAPNet also outperforms existing methods greatly on the new benchmarks.

1 Introduction

Semantic analysis of 3D scenes gains increasing popularity with the ubiquitous deployment of depth sensors, where point clouds are usually captured from the sensor fields of view as the most direct representation of 3D shapes. Among various tasks, classification of an input point cloud as one of a set of pre-defined object categories arguably plays the most fundamental role towards semantic understanding of the 3D scenes.

^{*}Contributed equally.

Research on 3D semantic analysis has largely been driven by preparation of benchmarking datasets [27, 2, 18, 7, 9]. For classification, representative methods such as PointNet [16], PointNet++ [17], and DGCNN [25] follows since the releasing of ModelNet [27] and ShapeNet [2]; for 3D detection (more precisely, 7 degrees-of-freedom object pose estimation), a plenty of methods have been proposed on KITTI [9], SUN-RGBD [18], ScanNet [7], and other benchmarks. Specific settings of these tasks usually follow the original definitions proposed with the benchmarks. Some of these settings could be in controlled, ideal conditions that deviate from those met in practice; consequently, algorithms ranking top on the benchmarks may not work well under practical conditions. For classification, for example, the benchmarking dataset of ModelNet40 [27] prepares its training and test instances of object point clouds under the *category-level, canonical poses* [12].¹ Even though such a problem setting is already challenging — the state-of-the-art methods on the ModelNet40 achieve $\sim 93\%$ accuracies only, researchers find that addressing the dataset challenges does not always translate as innovations useful for the practical problem of object point cloud classification, since some shortcut learning gives accuracies very close to the state-of-art ones, by identifying a sparse set of specially distributed but semantically less relevant points from each object point cloud [10]. The degenerate learning is (partially) caused by the less practical setups defined with the benchmarks, since learning setups closer to practical ones are more difficult to be hacked via shortcut learning [10].

More recently, the community realizes the less practical setups in existing benchmarks of object point cloud classification, and proposes rotation-augmented versions of these benchmarks by arbitrarily rotating their object instances [3, 8, 32]. They also propose strategies coping with the rotation arbitrariness, including implicitly learning object rotations in weakly supervised manners [16, 31], and extracting and learning rotation-invariant deep features [3, 32, 33]. However, the setups considered in these works are still one step away from the truly practical one, where due to (self-)occlusion, a captured point cloud covers *partial* surface of an object only, instead of the *complete* one considered in [27, 2]. Point cloud examples with three settings are compared and shown in the top row of Figure 1. In other words, the practical object point cloud classification is often under the *single-view, partial* setting. This subtle difference from complete to partial coverage of the object surface brings significant challenges to point cloud classification, as observed in Figure 1, where the performance of representative methods drops drastically under the single-view, partial setting. Indeed, the semantic category of an object point cloud is defined by its global, topological configuration of local shape primitives; a partial point cloud observed from an arbitrary view captures a subset of local shape primitives, whose classification is less ambiguous only when the distribution of partial point cloud on the whole surface is clearly specified.

We thus argue in this paper that, for effective classification of an arbitrarily posed, partial object point cloud, it is necessary to explicitly learn and predict its pose in the $SE(3)$ space. This technically means that an auxiliary task of *supervised* object pose learning should be accompanied with classification. To achieve the goal, we rely on steerable CNNs [6, 26] and propose a new architectural design termed *Pose-Accompanied Point cloud classification Network (PAPNet)*, whose pipeline is illustrated in Figure 2. The PAPNet starts with a backbone that processes an input point cloud of partial object surface with $SE(3)$ -equivariant convolutions, where pose-sensitive, equivariant features defined on

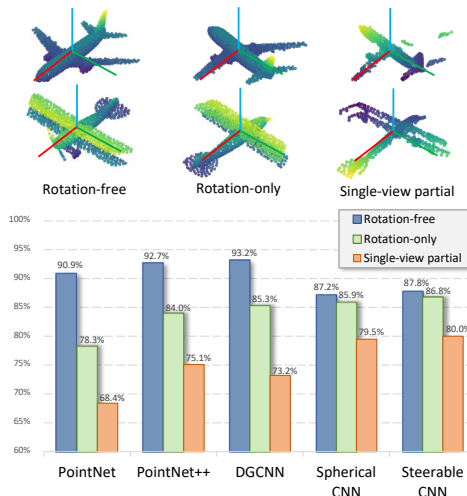


Figure 1: Top: Illustrative examples of the plane category from the ModelNet40 [27] with three settings; Bottom: comparative results of five popular point cloud classifiers, *i.e.* PointNet [16], PointNet++ [17], DGCNN [25], Spherical CNN [8], and 3D Steerable CNN [26], with three settings.

¹Intuitively speaking, one can think that a set of 3D *mug* models are under their category-level, canonical poses when their *handles* are aligned towards a same direction in the 3D space.

the vector fields of each layer are learned with the filters constructed from steerable basis kernels; on top of the backbone, we stack a pose estimator in parallel with classification header; a key design in our PAPNet is a transformation of the vector-field features at the backbone output using the predicted pose, such that classification can be (ideally) made in the canonical object pose; additionally, we use a category-dependent pose refiner that further enhances the classification. To test the efficacy of our design, existing benchmarks of object point cloud classification are adapted to the single-view, partial setting. Thorough experiments confirm the necessity of pose estimation for the considered practical setting of object point cloud classification, under which our method greatly outperforms existing ones. Main contributions are as follows.

- We approach object point cloud classification from a more practical perspective, and propose the single-view, partial setting under which point clouds covering the partial surface of object instances are observed. We discuss the limitations of existing methods, and show that their performance drops drastically under this practical setting.
- We propose a baseline method of Pose-Accompanied Point cloud classification Network (PAPNet)², which accompanies the classification task with an auxiliary one of supervised object pose learning. Built upon $SE(3)$ -equivariant convolutions, a key design in PAPNet is an intermediate transformation of vector-field features using the predicted pose, which eases the classification by (ideally) making it in the canonical pose space.
- To advance the research field, we adapt existing ModelNet40 and ScanNet benchmarks to the single-view, partial setting. Thorough experiments show the efficacy of our proposed PAPNet. Notably, the PAPNet greatly outperforms existing methods especially for more challenging noisy point clouds.

2 Related Works

In this section, we briefly review existing research that pursues object point cloud classification in practical, real-world conditions, and also the closely related research of object pose estimation. Discussions on the existing methods of point cloud classification under controlled conditions will be given in Section 4.

Towards Real-World Object Point Cloud Classification – Very few existing works [22, 31] have explored to handle with the compound challenges of rotation variations and partially visible shape. Uy *et al.* [22] propose a realistic point cloud classification benchmark, whose setting is similar to ours, but the main differences lie in two folds. On one hand, object shapes in the ScanObjectNN [22] only have arbitrary rotations along the vertical axis, instead of the $SO(3)$ rotation group containing all possible rotation transformations as our setting. On the other hand, point clouds in the ScanNet [7] and SceneNN [11] were obtained via fusion of a sequence of depth images with multiple viewpoints, and thus objects segmented by the ScanObjectNN [22] can not reflect single-view partiality in real data. Yuan *et al.* [31] share a similar observation on realistic point cloud classification to handle with partial and unaligned point clouds, but their weakly-supervised learning nature of spatial transformation can hardly guarantee canonical pose transformation (see Section 4).

Object Pose Estimation – The problem of 6D pose estimation aims to predict object poses (*i.e.* a rotation and translation) in camera space according to a canonical space. Existing 6D pose estimation can be categorized into two groups – instance-level [28, 14, 23, 29] and category-level [24, 4, 21]. In instance-level 6D pose estimation [28, 14, 23, 29], a typical assumption is adopted that CAD models for object instances to be estimated are available. In this sense, these methods concern more on learning to match partial observation to the CAD model. In category-level 6D pose estimation [24, 4, 21], CAD models of each instance are unavailable during training and testing. Such a problem is made more challenging to cope with shape variations of unseen object instances and thus relies on learning a high-quality category-level mean shape. The pose estimation task in our method falls into the latter group but without estimating the translation and size of object instances compared to existing category-level pose estimation methods, as negative effects of translation and size variations can be eliminated by normalizing the input point cloud to a unit ball in the classification task.

²<https://github.com/xzlskut/PartialPointClouds>

3 The Practical Problem of Object Point Cloud Classification

As two examples illustrated on the top-right of Figure 1, our considered practical setting assumes access to a point cloud $\mathcal{P} = \{\mathbf{p}_i \in \mathbb{R}^3\}_{i=1}^N \in \mathcal{X}$ covering *partial* surface of an object. Given a training set $\{\mathcal{P}_i, y_i\}_{i=1}^M$ of M instances, the task is to learn a classification model $\Phi : \mathcal{X} \rightarrow \mathcal{Y}$ that classifies any test \mathcal{P} into one of $K = |\mathcal{Y}|$ object categories. We define $\mathcal{Y} = \{1, \dots, K\}$ and $y_i \in \mathcal{Y}$ for any i^{th} training instance. As discussed in Section 1, to achieve effective point cloud classification under the single-view, partial setting, it is better to impose an auxiliary supervision for object pose estimation. This amounts to augmenting the training set as $\{\mathcal{P}_i, y_i, \mathbf{T}_i\}_{i=1}^M$, where the ground-truth pose $\mathbf{T}_i \in SE(3)$, $\mathbf{T} = [\mathbf{R}|\mathbf{t}]$ with rotation $\mathbf{R} \in SO(3)$ and translation $\mathbf{t} \in \mathbb{R}^3$, applies to \mathcal{P}_i in a point-wise manner and transforms \mathcal{P}_i into its canonical pose as $\mathbf{T}_i\mathcal{P}_i$. Note that the canonical pose of each \mathcal{P} is pre-defined at the category level, which can be obtained in a semi-automatic manner during preparation of training instances [12].

In contrast, existing methods either assume an *arbitrarily rotated, complete* point cloud $\tilde{\mathcal{P}} = \{\mathbf{p}_i \in \mathbb{R}^3\}_{i=1}^{\tilde{N}}$ covering the whole surface of an object [3, 32, 8], or assume $\mathbf{T}\tilde{\mathcal{P}}$ where \mathbf{T} rigidly transforms $\tilde{\mathcal{P}}$ into the category-level, canonical pose [16, 17, 25]. They correspondingly learn classification models using training sets of either $\{\tilde{\mathcal{P}}_i, y_i\}_{i=1}^M$ or $\{\mathbf{T}_i\tilde{\mathcal{P}}_i, y_i\}_{i=1}^M$. Note that in the latter case, $\{\mathbf{T}_i\}_{i=1}^M$ are implicitly assumed and are not used for classification learning; in other words, all the training and test instances have been pre-aligned into their canonical poses.

4 Existing Rotation-Agnostic Methods and Their Limitations

In this section, we discuss existing strategies for classification of *arbitrarily posed, complete* point clouds. Denote $\Phi_{fea} : \mathbb{R}^{\tilde{N} \times 3} \rightarrow \mathbb{R}^d$ as the feature encoding module, which produces d -dimensional feature embedding $\Phi_{fea}(\tilde{\mathcal{P}})$ for any input $\tilde{\mathcal{P}}$, and $\Phi_{cls} : \mathbb{R}^d \rightarrow [0, 1]^K$ as the final classifier typically constructed by fully-connected layers. These methods implement point cloud classification as a cascaded function $\Phi = \Phi_{cls} \circ \Phi_{fea}$.

Weakly Supervised Learning of Spatial Transformation – Given an arbitrarily posed input $\tilde{\mathcal{P}}$, a module Φ_{trans} parallel to Φ_{fea} is considered in [16, 25, 31] to predict a transformation $\hat{\mathbf{T}} = [\hat{\mathbf{R}}|\hat{\mathbf{t}}]$, which is then applied to $\tilde{\mathcal{P}}$ to reduce the variation caused by pose arbitrariness of $\tilde{\mathcal{P}}$. Learning of Φ_{trans} is conducted *in a weakly supervised manner*: classification supervision imposed on the network output of classifier Φ_{cls} propagates error signals back onto Φ_{trans} , whose updating is expected to improve the classification at the network output Φ_{cls} . Such a Φ_{trans} , termed T-Net, is proposed in [16], which is further improved as an iterative version in [31]; mathematically, let $\Delta\hat{\mathbf{T}}$ denote the predicted transformation update per iteration, and we have the transformation predicted at iteration t as a composition $\hat{\mathbf{T}}_t = \prod_{i=1}^t \Delta\hat{\mathbf{T}}_i$. Ideally, the predicted $\hat{\mathbf{T}}$ after a certain number of iterations are expected to transform $\tilde{\mathcal{P}}$ into its canonical pose, such that classification can be made easier on $\hat{\mathbf{T}}\tilde{\mathcal{P}}$; however, weakly supervised learning does not guarantee to achieve this, and in practice, the predicted $\hat{\mathbf{T}}$ is usually less relevant to canonical pose transformation.

Rotation-Invariant Feature Extraction and Learning – Rotation-invariant feature extraction requires that $[\Phi_{fea} \circ \Phi_{geo}](\mathbf{R}\tilde{\mathcal{P}}) = [\Phi_{fea} \circ \Phi_{geo}](\tilde{\mathcal{P}})$ for any $\mathbf{R} \in SO(3)$, where a module Φ_{geo} generates rotation-invariant geometric quantities. It can be easily verified that simple quantities such as point-wise norm and angle between a pair of points are rotation-invariant, *i.e.* $\|\mathbf{R}\mathbf{p}\|_2 = \|\mathbf{p}\|_2 \forall \mathbf{p} \in \mathbb{R}^3$ and $\langle \mathbf{R}\mathbf{p}, \mathbf{R}\mathbf{p}' \rangle = \langle \mathbf{p}, \mathbf{p}' \rangle \forall \mathbf{p}, \mathbf{p}' \in \mathbb{R}^3$. Rotation-invariant feature learning methods [3, 32, 30, 33] thus implement Φ_{fea} by learning point-wise features from these invariant outputs of Φ_{geo} , followed by pooling in a hierarchy of local neighborhoods constructed by graph networks [17, 25]. These methods may also be augmented with global pre-alignment of $\tilde{\mathcal{P}}$ (ideally) to the canonical pose, by computing the main axes of geometric variations of $\tilde{\mathcal{P}}$ via singular value decomposition [33]. We note that these invariant quantities only partially capture the geometric information contained in any $\tilde{\mathcal{P}}$; consequently, deep features learned from them would not be optimal for classification of $\tilde{\mathcal{P}}$.

Achieving Invariance via Learning Rotation-Equivariant Deep Features – Rotation invariance can also be achieved by first encoding the input into rotation-equivariant deep features and then converting the rotation-equivariant features into the rotation-invariant ones. Typical methods are spherical CNNs [5, 8]. Denote a rotation-equivariant layer as $\Psi : SO(3) \times \mathbb{R}^{d_{in}} \rightarrow SO(3) \times \mathbb{R}^{d_{out}}$; it processes an input signal $f : SO(3) \rightarrow \mathbb{R}^{d_{in}}$ with d_{out} layer filters, each of which is defined as $\psi : SO(3) \rightarrow \mathbb{R}^{d_{in}}$.³ Rotation-equivariant Ψ has the property $[\psi \star [\mathcal{T}_R f]](Q) = [\mathcal{T}'_R[\psi \star f]](Q)$, where $Q \in SO(3)$ and \mathcal{T}_R (or \mathcal{T}'_R) denotes a rotation operator that rotates the feature function f as $[\mathcal{T}_R f](Q) = f(R^{-1}Q)$, and \star denotes convolution on the rotation group; spherical convolution defined in [5, 8] guarantees achievement of the above property. A rotation-invariant Φ_{fea} can thus be constructed by cascading multiple layers of Ψ , followed by pooling the obtained features over the domain of $SO(3)$. To implement $\Phi_{fea}(\hat{\mathcal{P}})$, one may first cast each point $p \in \hat{\mathcal{P}}$ onto the unit sphere, with the accompanying point-wise geometry features (e.g. the length $\|p\|_2$), and then quantize the features to the closest grid of discrete sampling on the sphere. Due to numerical approximations and the use of nonlinearities between layers, the encoder based on spherical CNNs is not perfectly rotation-equivariant, which affects the rotation invariance of features obtained by the subsequent pooling [19]. Alternative manners [20, 26] exist that directly learn rotation-equivariant point-wise filters based on steerable basis kernels in the Euclidean domain.

4.1 Limitations of Existing Methods under the Single-View, Partial Setting

The aforementioned existing methods are originally proposed for classifying point clouds sampled from complete object surfaces; nevertheless, one might be tempted to apply them to the single-view, partial setting considered in the present paper. However, we will analyze that the simple change of settings from complete to partial surfaces brings significant challenges to classification, and may cause either failure or severe performance degradation of the above methods. Indeed, as discussed in Section 1, semantics of object point clouds are defined by global configurations of local shape primitives; a partial object surface observed from an arbitrary view captures a subset of local shape primitives only, which makes it difficult to specify some semantics that can be clearly defined only when the global configurations are available.

More specifically, for methods [16, 25, 31], the learned \hat{T} via training Φ_{trans} in a weakly supervised manner becomes even less relevant to canonical pose transformation when the input is a point cloud \mathcal{P} of partial surface; for both the methods using rotation-invariant feature extraction [3, 32, 30, 33] and those achieving invariance by pooling over learned rotation-equivariant deep features [5, 8, 20, 26], a partial \mathcal{P} observed from an arbitrary view is ambiguous for specifying how such a \mathcal{P} is configured globally on the whole surface, and consequently classifiers would be confused between the global and local levels. In addition, we note that pre-alignment of a partial \mathcal{P} via computation of main geometric axes easily causes misalignments.

Figure 1 verifies the above analysis empirically. More comprehensive experiments are presented in Section 6. Given the limitations of existing methods for the practical challenge of object point cloud classification under the single-view, partial setting, we argue that an explicit, *supervised learning* of object pose from the observed partial point cloud is necessary.

5 Pose-Accompanied Point Cloud Classification Network (PAPNet)

As mentioned in Section 1, the global configurations of local shape primitives are desired to specify semantic patterns when only single-view partial point clouds available, which thus encourages an auxiliary task of supervised regression on object poses to accompany object point cloud classification.

5.1 $SE(3)$ -equivariant Convolution Based on Steerable Basis Kernels

Our PAPNet relies on the 3D steerable convolution proposed in [26], which guarantees that rigid transformations of objects in the Euclidean space can lead to an equivalent transformation of features in feature space. To this end, features $f(v) \in \mathbb{R}^{d_l}$ on position $v \in \mathbb{R}^3$ of layer l is represented by a

³Note that both f and ψ , and the filtered responses are defined on the domain of rotation group $SO(3)$; when the layer is the network input, f and ψ are defined on the domain of a sphere S^2 .

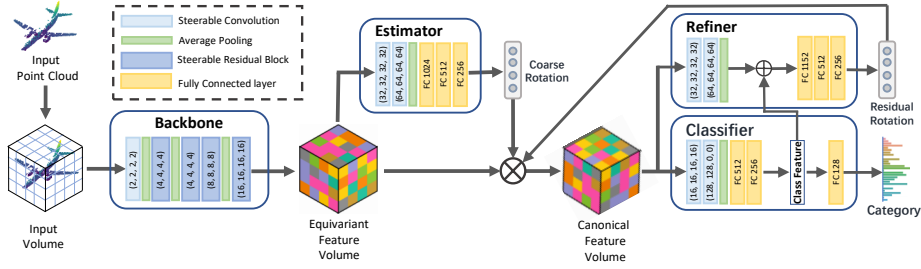


Figure 2: Pipeline of our PAPNet on classifying partial point sets with an auxiliary prediction of object pose. The channels of steerable convolution and residual block can be represented by a tuple of numbers, where the position denotes the order of the irreducible features and the corresponding value is the number of features of that order.

set of scalar-valued and vector-formed geometrical quantities, where function $\mathbf{f} : \mathbb{R}^3 \rightarrow \mathbb{R}^{d_l}$ defines the feature space \mathcal{F}_l as a combination of multiple scalar and vector fields.

Each geometrical quantity field transforms independently under rigid body motion $\mathbf{T} = [\mathbf{R}|\mathbf{t}]$ as:

$$[\mathcal{T}(\mathbf{T})\mathbf{f}](\mathbf{v}) := \rho_l(\mathbf{R})\mathbf{f}(\mathbf{R}^{-1}(\mathbf{v} - \mathbf{t})), \quad (1)$$

where \mathcal{T} denotes the transformation operator and ρ_l is a representation of $SO(3)$ which describes the rotation behavior of fields in layer l . Since the translation of the observed point cloud can be approximated well by its coordinate mean in the classification task. We translate the observed point cloud to the origin by its coordinate mean and simplify the transformation law in feature space with only rotation \mathbf{R} as follows:

$$[\mathcal{T}_{\mathbf{R}}(\mathbf{R})\mathbf{f}](\mathbf{v}) := \rho_l(\mathbf{R})\mathbf{f}(\mathbf{R}^{-1}\mathbf{v}), \quad (2)$$

where $\mathcal{T}_{\mathbf{R}}$ denotes the rotation operator.

Any representation of $SO(3)$ can be constructed from irreducible representation of dimension $2k + 1$, for $k = 0, 1, 2, \dots, \infty$, which is known as the Wigner-D matrix $D^k(\mathbf{R})$ of order k [26]. The $SO(3)$ representation in layer l can thus be written as:

$$\rho_l(\mathbf{R}) = \mathbf{Q}^{-1} \left[\bigoplus_{i=1}^{\mathcal{F}_l} D^{k_i}(\mathbf{R}) \right] \mathbf{Q}, \quad (3)$$

where \bigoplus denote the construction of a block-diagonal matrix with blocks $D^{k_i}(\mathbf{R})$, and \mathbf{Q} is a change of basis matrix. As a result, the $SO(3)$ -equivariant features in layer l is a stack of F_l features $f^i(\mathbf{v}) \in \mathbb{R}^{2k_i+1}$, so that $d_l = \sum_{i=1}^{\mathcal{F}_l} (2k_i + 1)$.

In [26], Weiler *et al.* derived analytically that the equivariant convolutional kernel between adjacent feature spaces must satisfy the kernel constraint:

$$\kappa(\mathbf{R}\mathbf{v}) = \rho_{l+1}(\mathbf{R})\kappa(\mathbf{v})\rho_l(\mathbf{R})^{-1}, \quad (4)$$

where $\kappa : \mathbb{R}^3 \rightarrow \mathbb{R}^{d_{l+1} \times d_l}$ is the convolutional kernel. The solution space formed by this linear constraint can be spanned by the steerable basis kernels [26]. Consequently, equivariant convolutional kernel built up by linearly combining these steerable basis kernels using learnable weights guarantee that features in layer $l + 1$ transform according to $\rho_{l+1}(\mathbf{R})$ if features in layer l transform according to $\rho_l(\mathbf{R})$.

5.2 Network Architecture

Dependent on 3D steerable convolutions [26], we introduce a novel network architectural design, which is shown in Figure 2. Specifically, the proposed PAPNet consists of four modules: one steerable convolutional backbone, one pose estimator, one classification module, and one class-dependent pose refiner. With the voxelized representation of a point cloud \mathcal{P} from partial object surface as input, the backbone network processes to generate the rotation-equivariant features \mathbf{f} which consist of scalar fields and vector fields. The output features of the backbone are fed into the pose estimator, whose predictions $\hat{\mathbf{R}}$ enforce explicitly alignment of the vector-field features of the backbone into

the category-level canonical pose. As a result, negative effects of rotation arbitrariness and feature variations on point cloud classification can be mitigated in the pose-aligned vector-field feature space. To further cope with feature inconsistency caused by inaccurate poses, the refiner is developed to refine category-correlated pose predictions in a residual learning manner.

Backbone – The backbone module contains nine steerable convolutional layers in addition to three average pooling layers, as shown in Figure 2. Beyond the first steerable convolutional layer, the remaining ones are divided into four blocks. Each block contains two convolutional layers and a residual shortcut across layers. Such a shared backbone encodes the input into an equivariant feature volume $\mathbf{f} : \mathbb{R}^3 \rightarrow \mathbb{R}^d$ where the feature vector $\mathbf{f}(\mathbf{v}) \in \mathbb{R}^d$ anchored on each voxel $\mathbf{v} \in \mathbb{R}^3$ is made up of multiple scalars and high-dimensional vectors.

Pose Estimation Branch – The pose estimator comprises two steerable convolution layers followed by three fully connected (FC) layers. The equivariant feature volume generated by the backbone is fed into the pose estimator to produce a coarse rotation $\hat{\mathbf{R}}$ which can be formulated into a quaternion $\hat{\mathbf{q}}$. The rotation prediction $\hat{\mathbf{R}}$ can be used to transform the equivariant feature \mathbf{f} under the camera space to approach its canonical space by Eqn (2), where we obtain aligned feature $\mathbf{f}_c = \mathcal{T}_{\mathbf{R}}(\hat{\mathbf{R}}^{-1})\mathbf{f}$ by coarse pose $\hat{\mathbf{R}}$.

Classification on Equivariant Features – Similar to the pose estimator, the classifier consists of two steerable convolution layers and three FC layers. 3D steerable CNN [26] achieves rotation-invariance by converting all rotation-equivariant vector fields into rotation-invariant scalar fields before pooling over the Euclidean space. Different from [26], our PAPNet transforms the pose-sensitive vector-field features to their canonical pose as input of the classifier and pools the canonical vector fields in the last steerable convolutional layer of the classifier to obtain a pose-insensitive global feature while preserving discrimination of high-dimensional vector features. Our motivation lies in that, after transformation on equivariant vector fields, feature learning under the category-level canonical space can be made easier in view of less semantic ambiguity on local object shape.

Category-Aware Pose Refining – The pose feature encoded by two convolutional layers of the refiner is concatenated with the feature from the classifier to predict a residual rotation $\Delta\hat{\mathbf{R}}$ which is in the quaternion form of $\Delta\hat{\mathbf{q}}$. $\Delta\hat{\mathbf{R}}$ can enforce the pose-aligned features further approaching its canonical space by $\mathbf{f}'_c = \mathcal{T}_{\mathbf{R}}(\Delta\hat{\mathbf{R}}^{-1})\mathbf{f}_c$. In this manner, superior classification performance can be achieved, in light of less feature variations with more accurate pose predictions.

Loss Functions – In our scheme, for each point cloud instance \mathcal{P} , we have two types of supervision signals – the class label \mathbf{y} and the pose label \mathbf{q} converted from $\mathbf{R} \in SO(3)$. For supervising the model of pose estimation, we employ the loss based on the Euclidean norm as follows:

$$L_{\text{pos}} = \|\mathbf{q} - \hat{\mathbf{q}}\| + \|\mathbf{q} - \hat{\mathbf{q}} \circ \Delta\hat{\mathbf{q}}\| \quad (5)$$

where $\hat{\mathbf{q}}$ and $\Delta\hat{\mathbf{q}}$ are the coarse and residual quaternion-formed rotation predictions generated by the estimator and refiner respectively, and \circ denotes the Hamilton product. Moreover, object symmetry is an inevitable problem for pose estimation, as there exists a large number of objects with continuous symmetry or discrete symmetry, *e.g.* bottle, dresser and glass box in the ModelNet40, we use the method proposed in [15] to map ambiguous rotations to an unambiguous one. For the classification loss L_{cls} , the typical cross entropy loss [16, 25] is used. In general, the total loss of our PAPNet can be written as:

$$L_{\text{total}} = L_{\text{cls}} + \lambda L_{\text{pos}} \quad (6)$$

where λ is a trade-off parameter between the classification and pose losses.

6 Experiments

6.1 Generation of Single-View Partial Point Cloud Datasets

Very few works have explored to generate and release benchmarks of arbitrarily-posed partial point cloud classification, but the available datasets [27, 22] lacks object pose annotations, which thus fails to specify the configuration of partial shape on the object surface. In light of this, we adapt the popular synthetic ModelNet40 [27] and realistic ScanNet [7] to the single-view partial setting with several examples illustrated in Figure 3.

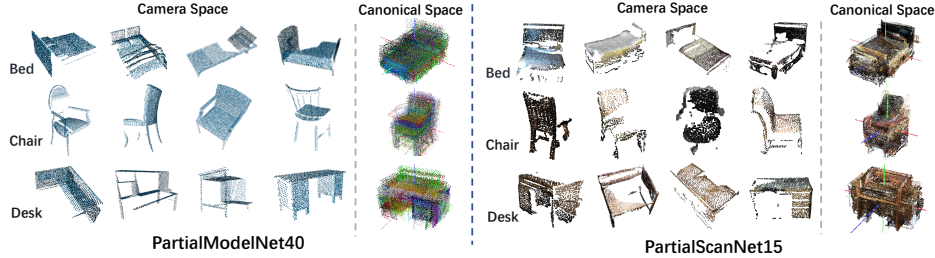


Figure 3: Illustration of the PartialModelNet40 and PartialScanNet15 datasets adapted from the ModelNet40 [27] and ScanNet [7].

PartialModelNet40 – The ModelNet40 [27] contains 12,311 CAD models belonging to 40 semantic categories which are split into 9,843 for training and 2,468 for testing. For the PartialModelNet40, we randomly sampled rotation and translation on $SO(3)$ within $t_x, t_y \sim \mathcal{U}(-2.0, 2.0)$, $t_z \sim \mathcal{U}(2.0, 5.0)$, and rendered ten depth images with corresponding pose labels for each training instance in the ModelNet40. These depth images are converted into partial point clouds using the intrinsic parameters of a virtual camera. The testing set is constructed by randomly sampling one depth image of each testing instance of the ModelNet40 under one arbitrary view. In general, the PartialModelNet40 contains 98,430 training samples and 2,468 testing samples.

PartialScanNet15 – The ScanNet [7] contains 1513 scanned and reconstructed real-world indoor scenes. We selected 15 categories with a sufficient number of instances in the scenes, and segmented and collected those instances using provided bounding boxes and semantic labels. With the pose annotations provided by Scan2CAD [1], the segmented point cloud is first aligned to the canonical space, from which point cloud instances are sampled along with ten randomly selected viewpoints. These point clouds are then transformed into the camera coordinate system. Since the original ScanNet is generated by fusing a sequence of depth scans and object shapes segmenting from the ScanNet contain redundant surface observed from multiple views, we employ hidden point removal (HPR) [13] to filter out the invisible points due to self-occlusion under a single perspective. In total, our PartialScanNet15 contains 22,670 training samples and 5,650 test samples belonging to 15 categories. The PartialScanNet15 is challenging in view of the existence of realistic sensor noises, nonuniform densities, various poses, and partiality due to self-occlusion and occlusions in the cluttered context.

6.2 Settings

Comparative Methods – We compare representative point classifiers and a number of rotation-agnostic methods investigated in Section 4 with the proposed PAPNet. The spatial transformation network (TNet) [16] and iterative transformation network (ITNet) [31] are adopted as an explicit spatial transformation module. For learning rotation-invariant feature representation, we choose the rigorously rotation-invariant (RRI) representation proposed in ClusterNet [3], which can achieve the state-of-the-art performance with a solid theoretical guarantee. TNet, ITNet, and RRI are all followed by conventional PointNet++ (PN++) for feature encoding and classification, owing to its best performance among rotation-sensitive point classifiers (see Table 1). We use the Spherical CNN [8] and (3D) steerable CNN [26] as competing rotation-equivariant methods. The direct competitor is the steerable CNN, which shares the identical backbone and classifier modules with our PAPNet, but replaces the last steerable convolution channel from $(128, 128, 0, 0)$ with $(512, 0, 0, 0)$ to achieve rotation-invariance on scalar fields. For a fair comparison, all methods use the same 1024 points as input. We follow the default parameters and training strategies of comparative methods suggested in the paper. For performance evaluation, the average precision of object instances for which the angular distance less than 10° [24, 21] and classification accuracy [16, 17] are adopted for pose estimation and point cloud classification respectively.

Implementation Details – To train our model, we adopt the Adam optimizer with a learning rate of 0.005. Since the convergence speed of pose estimation is much slower than that of classification, we first trained the backbone and estimator for 20 epochs, then activated the classifier to train 15 epochs, and finally activated the refiner to train another 15 epochs. The hyper-parameter λ between classification loss and pose loss in Eqn (6) was set as 0.1 which was optimally selected from

Table 1: Comparative evaluation on classification accuracy (%) with the PartialModelNet40 and the PartialScanNet15. The last row is the transferability evaluation from the PartialModelNet40 to the PartialScanNet15.

	PointNet	DGCNN	PointNet++	TNet-PN++	ITNet-PN++	RRI-PN++	Spherical CNN	Steerable CNN	PAPNet (ours)	PAPNet (oracle)
Input (size)	1024	1024	1024	1024	1024	1024	1×64^2	1×64^3	1×64^3	1×64^3
PartialModelNet40	65.8%	73.2%	75.1%	75.7%	75.7%	77.2%	79.5%	80.0%	81.9%	87.2%
PartialScanNet15	68.4%	76.4%	78.2%	79.0%	79.2%	83.0%	85.2%	85.5%	88.7%	93.4%
Transferability	35.0%	34.4%	29.0%	29.4%	30.1%	39.8%	44.2%	48.5%	53.7%	N/A

{0.01, 0.1, 0.5, 1.0, 5.0}. Our method contains a total of 1.9M parameters, which is comparable with other comparative methods (0.5M - 3.6M parameters).

6.3 Results

Comparative Evaluation – We compare our PAPNet with competing methods on both datasets, whose results are shown in Table 1. Our method gains at least 1.9% and 3.2% improvement on classification accuracy over other methods on the PartialModelNet40 and PartialScanNet15 respectively. Such an observation demonstrates learning from consistent geometries under the canonical space can mitigate suffering from feature inconsistency with pose variation and partiality. More importantly, the proposed PAPNet can perform more robustly than other methods on noisy point clouds of the more challenging PartialScanNet15, owing to effectively alleviating feature inconsistency via an auxiliary pose estimation. In general, all rotation-sensitive classifiers, *i.e.* PointNet, DGCNN and PointNet++, are outperformed by all rotation-agnostic methods, under the single-view partial setting. More specifically, both TNet and ITNet can only slightly outperform the baseline PointNet++, indicating that weak supervision on pose transformation can hardly tackle the pose variation in the single-view partial setting. Spherical CNN and Steerable CNN have better performance than RRI-PN++, which can be explained by geometric information missed by rotation-invariant quantities can be optimally discovered in equivariant feature encoding. Our method incorporates an auxiliary supervised pose estimation based on the Steerable CNN, which further improves its results. The oracle method in Table 1 reports the results of our PAPNet replacing the pose predictions with ground-truth poses for canonical feature alignment, which can be the upper bound of our method.

Ablation Study – We evaluate two degenerated methods to simultaneously classify partial point clouds and estimate pose, which are the more fair comparison with the proposed PAPNet in the perspective of the usage of both pose and class supervision, whose results are shown in Figure 2. The first method is designed in a popular multi-task learning structure, which shares a backbone and two header branches on top of the backbone. Such a method (multi-task learning in Table 2) can hardly improve classification performance, which can be caused by the steerable basis kernels in the backbone fails to capture rotation-sensitive information desired in pose estimation and achieve rotation-invariance in classification simultaneously. Furthermore, the only difference between our PAPNet and the other degenerated variant lies in whether the model rigidly transforms the input or the intermediate equivariant features to the canonical space. Our PAPNet performs better than the method using input transformation, in view of conflict of equivariant feature encoding of the shared backbone under arbitrary camera view in the pose estimation task and canonical view in the classification task. Both experiments can verify the rationale of the network structure of PAPNet. Moreover, as shown in Table 2, the PAPNet aligns 50.3% of the testing samples on PartialModelNet40 to their canonical pose. Symmetry processing and pose refinement are verified their effectiveness, which improve pose accuracy by 19.5% and 18.5% and classification accuracy by 0.7% and 0.9%.

Evaluation of Transferability – To evaluate cross-dataset transferability, samples belong to the 12 common classes of both datasets are used. As shown in the bottom line of Table 1, the voxel-based rotation equivariant methods generalize consistently better than those MLP-based point cloud classifiers. Our PAPNet achieves the best performance, which further demonstrates the effectiveness of the introduction of supervised pose regression on alleviating semantic ambiguity even with significant domain discrepancy on point distribution.

Table 2: Ablation study of our proposed model.

	Multi-task Learning	Input Transformation	w/o Symmetry	w/o Refinement	PAPNet
Pose Acc	11.1%	29.5%	30.8%	31.8%	50.3%
Classification Acc	79.7%	80.3%	81.2%	81.0%	81.9%

7 Conclusion

This paper introduces a practical perspective of classification of object point clouds, which desires global configurations to alleviate semantic ambiguity. To this end, a novel classification network accompanied with supervised pose regression is proposed, which can beat exiting rotation-agnostic methods and two degenerated variants. The superior performance of the proposed method can be credited to make classification easier via explicit rigid transformation of equivariant vector-field features to the canonical space. The contributed scheme might be under adversarial attacks, causing total failure of the whole perception system, which encourages academic researchers and safety engineers to mitigate these risks.

References

- [1] A. Avetisyan, M. Dahnert, A. Dai, M. Savva, A. X. Chang, and M. Nießner. Scan2cad: Learning cad model alignment in rgb-d scans. *CVPR*, 2019.
- [2] A. X. Chang, T. Funkhouser, L. Guibas, P. Hanrahan, Q. Huang, Z. Li, S. Savarese, M. Savva, S. Song, H. Su, J. Xiao, L. Yi, and F. Yu. Shapenet: An information-rich 3d model repository. *ArXiv*, 2015.
- [3] C. Chen, G. Li, R. Xu, T. Chen, M. Wang, and L. Lin. Clusternet: Deep hierarchical cluster network with rigorously rotation-invariant representation for point cloud analysis. In *CVPR*, 2019.
- [4] D. Chen, J. Li, and K. Xu. Learning canonical shape space for category-level 6d object pose and size estimation. *CVPR*, 2020.
- [5] T. Cohen, M. Geiger, J. Köhler, and M. Welling. Spherical cnns. *ArXiv*, 2018.
- [6] Taco Cohen and M. Welling. Steerable cnns. *ArXiv*, 2017.
- [7] A. Dai, A. X. Chang, M. Savva, M. Halber, T. Funkhouser, and M. Nießner. Scannet: Richly-annotated 3d reconstructions of indoor scenes. *CVPR*, 2017.
- [8] C. Esteves, C. Allen-Blanchette, A. Makadia, and K. Daniilidis. Learning so(3) equivariant representations with spherical cnns. In *ECCV*, 2018.
- [9] A. Geiger, P. Lenz, and R. Urtasun. Are we ready for autonomous driving? the kitti vision benchmark suite. In *CVPR*, 2012.
- [10] Robert Geirhos, Jörn-Henrik Jacobsen, Claudio Michaelis, Richard Zemel, Wieland Brendel, Matthias Bethge, and Felix A Wichmann. Shortcut learning in deep neural networks. *Nature Machine Intelligence*, 2020.
- [11] B. S. Hua, Q. H. Pham, D. Nguyen, M. Tran, L. F. Yu, and S. Yeung. Scenenn: A scene meshes dataset with annotations. *3DV*, 2016.
- [12] Qixing Huang, Hao Su, and L. Guibas. Fine-grained semi-supervised labeling of large shape collections. *ACM Transactions on Graphics (TOG)*, 2013.
- [13] S. Katz, A. Tal, and R. Basri. Direct visibility of point sets. *TOG*, 2007.
- [14] Y. Li, G. Wang, X. Ji, Y. Xiang, and D. Fox. Deepim: Deep iterative matching for 6d pose estimation. *IJCV*, 2019.
- [15] G. Pitteri, M. Ramamonjisoa, S. Ilic, and V. Lepetit. On object symmetries and 6d pose estimation from images. *3DV*, 2019.
- [16] C. R. Qi, H. Su, K. Mo, and L. J. Guibas. Pointnet: Deep learning on point sets for 3d classification and segmentation. *CVPR*, 2016.
- [17] C. R. Qi, L. Yi, H. Su, and L. J. Guibas. Pointnet++: Deep hierarchical feature learning on point sets in a metric space. *NeurIPS*, 2017.
- [18] S. Song, S. P. Lichtenberg, and J. Xiao. Sun rgb-d: A rgb-d scene understanding benchmark suite. *CVPR*, 2015.
- [19] R. Spezialetti, S. Salti, and L. D. Stefano. Learning an effective equivariant 3d descriptor without supervision. In *ICCV*, 2019.
- [20] N. Thomas, T. Smidt, S. M. Kearnes, L. Yang, L. Li, K. Kohlhoff, and P. Riley. Tensor field networks: Rotation- and translation-equivariant neural networks for 3d point clouds. *ArXiv*, 2018.

- [21] M. Tian, M. Ang, and G. H. Lee. Shape prior deformation for categorical 6d object pose and size estimation. In *ECCV*, 2020.
- [22] M. A. Uy, Q. H. Pham, B. S. Hua, D. Nguyen, and S. Yeung. Revisiting point cloud classification: A new benchmark dataset and classification model on real-world data. *ICCV*, 2019.
- [23] C. Wang, D. Xu, Y. Zhu, R. Martín-Martín, C. Lu, L. Fei-Fei, and S. Savarese. Densefusion: 6d object pose estimation by iterative dense fusion. *CVPR*, 2019.
- [24] H. Wang, S. Sridhar, J. Huang, J. Valentin, S. Song, and L. Guibas. Normalized object coordinate space for category-level 6d object pose and size estimation. *CVPR*, 2019.
- [25] Y. Wang, Y. Sun, Z. Liu, S. Sarma, M. Bronstein, and J. Solomon. Dynamic graph cnn for learning on point clouds. *TOG*, 2019.
- [26] M. Weiler, M. Geiger, M. Welling, W. Boomsma, and T. Cohen. 3d steerable cnns: Learning rotationally equivariant features in volumetric data. In *NeurIPS*, 2018.
- [27] Z. Wu, S. Song, A. Khosla, F. Yu, L. Zhang, X. Tang, and J. Xiao. 3d shapenets: A deep representation for volumetric shapes. *CVPR*, 2015.
- [28] Y. Xiang, T. Schmidt, V. Narayanan, and D. Fox. Posecnn: A convolutional neural network for 6d object pose estimation in cluttered scenes. *ArXiv*, 2018.
- [29] Z. Xu, K. Chen, and K. Jia. W-poseNet: Dense correspondence regularized pixel pair pose regression. *ArXiv*, 2019.
- [30] Y. You, Y. Lou, Q. Liu, Y. Tai, L. Ma, C. Lu, and W. Wang. Pointwise rotation-invariant network with adaptive sampling and 3d spherical voxel convolution. In *AAAI*, 2020.
- [31] W. Yuan, D. Held, C. Mertz, and M. Hebert. Iterative transformer network for 3d point cloud. *ArXiv*, 2018.
- [32] Z. Zhang, B. Hua, D. W. Rosen, and S. Yeung. Rotation invariant convolutions for 3d point clouds deep learning. In *3DV*, 2019.
- [33] C. Zhao, J. Yang, X. Xiong, A. Zhu, Z. Cao, and X. Li. Rotation invariant point cloud classification: Where local geometry meets global topology. *ArXiv*, 2019.